A model of extravascular bubble evolution: effect of changes in breathing gas composition

J. F. HIMM AND L. D. HOMER
Naval Medical Research Institute, Bethesda, Maryland 20889-5607

Himm, J. F., and L. D. Homer. A model of extravascular bubble evolution: effect of changes in breathing gas composition. *J. Appl. Physiol.* 87(4): 1521–1531, 1999.—Observations of bubble evolution in rats after decompression from air dives (O. Hyldegaard and J. Madsen. *Undersea Biomed. Res.* 16: 185–193, 1989; O. Hyldegaard and J. Madsen. *Undersea Hyperbaric Med.* 21: 413–424, 1994; O. Hyldegaard, M. Moller, and J. Madsen. *Undersea Biomed. Res.* 18: 361–371, 1991) suggest that bubbles may resolve more safely when the breathing gas is a heliox mixture than when it is pure O_2. This is due to a transient period of bubble growth seen during switches to O_2 breathing. In an attempt to understand these experimental results, we have developed a multigas-multipressure mathematical model of bubble evolution, which consists of a bubble in a well-stirred liquid. The liquid exchanges gas with the bubble via diffusion, and the exchange between liquid and blood is described by a single-exponential time constant for each inert gas. The model indicates that bubbles resolve most rapidly in spinal tissue, in adipose tissue, and in aqueous tissues when the breathing gas is switched to O_2 after surfacing. In addition, the model suggests that switching to heliox breathing may prolong the existence of the bubble relative to breathing air for bubbles in spinal and adipose tissues. Some possible explanations for the discrepancy between model and experiment are discussed.

gas bubble evolution; breathing gas change; inert gas; countercurrent exchange; oxygen

THE LEADING CANDIDATE in the etiology of decompression sickness (DCS) is the evolution of gas bubbles in the tissues and circulatory system of the diver, at least in cases where symptoms appear shortly after surfacing (3). Numerous investigators have developed models of bubble evolution in tissue (2, 6, 22, 32), and some work has been done in modeling bubble evolution in blood vessels (12a). In addition, bubble-related models have been important in the development of decompression procedures at the University of Pennsylvania (9), the Naval Medical Research Institute (25a, 26, 36), and the Defence and Civilian Institute of Environmental Medicine (30). However, few of the models have been validated experimentally (34). The recent observations by Hyldegaard et al. (16, 17, 19) of the growth and dissolution of bubbles in rats after decompression from an air dive offer an opportunity to validate some of these models.

The first series of experiments performed by Hyldegaard and Madsen (16) looked at the effect of breathing gas switches on the evolution of gas bubbles in adipose tissue after a dive to ~75 feet seawater (fsw) for 4 h. The bubbles observed in the fat tissue developed naturally as a consequence of the dive and were not introduced into the tissue by the investigators. Observations of the bubbles began ~30 min after decompression, and switches in the breathing gas occurred during the following 30 min. Bubbles grew in rats that continued to breathe air throughout the observation period. When the breathing gas was switched to a heliox mixture, bubbles consistently diminished in size; when the breathing gas was switched to pure O_2, bubbles resolved in about the same time frame as during heliox breathing. The initial response to the O_2 breathing was a stabilization or growth of the bubble, followed by a more rapid resolution of the bubble than was seen during the heliox breathing. One bubble continued to grow throughout the O_2 breathing. If the breathing mixture was switched a second time from heliox to air or N_2O-O_2 while the bubble was still of an appreciable size, the bubble would resume growing.

The second series of experiments (19) involved bubbles injected into the white matter of the spine after a 4-h dive to 70 fsw. Results for this series of experiments were similar to those in which bubbles were injected into the adipose tissue. Most bubbles grew throughout the observation period, whereas heliox or O_2 breathing led to a resolution of the bubble. Again, O_2 breathing caused an initial growth of the bubble, followed by a more rapid dissolution than was seen during heliox breathing. A second breathing gas switch to N_2O-O_2 while the bubble was still appreciable in size led to resumed growth of the bubble.

The third series of experiments (17) involved bubbles injected into muscle and tendon after a 1-h dive to 80 fsw. The effect of the breathing gas switches on the injected bubbles was similar in muscle and tendon. Bubbles resolved rapidly after the switch. Continued breathing of air led to a period of growth for bubbles in muscle tissue, whereas bubbles diminished steadily after injection into tendon.

Initial bubble diameters were highly variable; spinal bubbles were roughly 300 μm; and adipose, muscle, and tendon bubbles were ~600 μm. Bubbles that resolved

typically did so within ~3 h in spinal and adipose tissues and within ~4 h in muscle and tendon.

Thus the experiments of Hyldegaard et al. (16, 17, 19) indicate that changes in breathing gas composition can affect the time course of bubble evolution. Bubbles resolve more rapidly when the breathing gas is switched to 80% He-20% O_2 or 100% O_2 than with air breathing after surfacing. Bubbles resolved more slowly, or not at all, when air was the breathing gas. Bubbles in adipose tissue, spinal white matter, and tendon could undergo a transient period of growth after the breathing gas was switched to pure O_2. Such growth was not observed after the breathing gas was switched to heliox. On the basis of these results (and on the standard assumption that DCS is alleviated by eliminating bubbles), the Israeli Navy has modified its DCS treatment procedure by recompressing patients on He-O_2 instead of pure O_2 in cases where neurological symptoms are manifested (23; A. Shupak, personal communication).

To determine the relative importance of various physiological factors in the evolution of a bubble in tissue, we have developed a detailed model of bubble evolution in a liquid. The specific aim is to test whether one should expect the breathing of certain gases to be inherently advantageous in helping resolve extravascular bubbles or whether certain sequences of "gas switches" are advantageous. When dives similar to those performed by Hyldegaard et al. (16, 17, 19) are simulated, several discrepancies between the bubble model and the experimental results arise with the assumption of normal physiological parameters for the rat tissues. Possible sources of the discrepancies, including altered tissue perfusion, altered O_2 consumption in the tissue, and countercurrent exchange (CCE) of the inert breathing gases, are explored with use of the model.

DESCRIPTION OF THE MODEL

Here we discuss the assumptions on which the model is based. The translation of those assumptions into equations is shown in the APPENDIX.

The model describes a spherical bubble in a homogeneous liquid of finite volume. The bubble exchanges gas with the surrounding liquid at a finite rate. The rate is computed using the steady-state mass transfer coefficient for a sphere in a stagnant liquid, although the system is unsteady state. This approximation is adequate only when the transport rate and the rate of change of the bubble radius are sufficiently slow. Therefore, the model is expected to give a poor description of bubble dynamics during rapid changes of hydrostatic pressure or when the bubble is "small" (i.e., $\sigma/R >$ 25,000 dyn/cm^2, where σ is surface tension and R is bubble radius).

The dissolved gases are uniformly distributed throughout the liquid; i.e., it behaves as a well-mixed compartment. The liquid is equilibrated with a third phase that flows past it. For our purposes, the liquid can be thought of as a volume of tissue being perfused by blood. The assumption that the tissue and blood are equilibrated means that when Henry's law is obeyed in tissue and blood, the rate of gas exchange between them is governed by the familiar single-exponential kinetic model. Single-exponential kinetics, therefore, are used for the inert gases N_2 and He and for CO_2, but not for O_2, the solubility of which in blood does not follow ideal solution behavior because of binding to Hb. Although CO_2 also binds to Hb, its high effective solubility in tissue (see APPENDIX) leads to a virtually constant tissue partial pressure of 0.0461 ATA under all conditions explored here, so the simpler single-exponential kinetics were used.

The effects of CCE are taken into account by requiring that the concentration of an inert gas in the arterial blood supplied to the tissue be between the concentration in the arterial blood in the lung and the concentration in the tissue. The CCE process has a greater effect on inert gas exchange for the more diffusible gases.

Because the process of bubble nucleation is not understood, a bubble that does not exchange gas with the surrounding tissue is assumed to be present at the start of the dive. During decompression the bubble begins to exchange gas with the surrounding tissue when the sum of partial pressures of the gases in the tissue exceeds the sum of the partial pressures of these same gases in the bubble. If the rate of decompression is slow enough, this partial pressure condition will not be met, and the bubble will not evolve.

The assumption of uniformity within the tissue volume might be the most unsatisfactory one that we are forced to make. On the one hand, the bubble is treated as being in a quiescent fluid for the purpose of calculating gas flux across the interface. This is consistent with the properties of a tissue, where the fluid content of the tissue is bound within cells. On the other hand, the tissue is assumed to be well stirred because of the convective flow of the blood. In addition, not only has it been shown experimentally (25) and via simulation (14) that inert gas kinetics in muscle are not simply described, this assumption also precludes the inclusion of potentially important geometry-specific information, e.g., the distance from the bubble to the nearest blood vessels. A more complete treatment of the tissue might be attempted, but there are too many unknowns regarding the interaction of a bubble with the tissue. Direct effects of the bubble include possible changes in the blood flow in the smaller vessels near the evolving bubble, the accumulation of surfactants at the tissue-bubble interface interfering with the transport of gases into and out of the bubble, and the contribution of tissue elasticity to the internal bubble pressure. Indirect effects may include the triggering of the immune system, leading to changes in perfusion and O_2 consumption, as well as swelling of the tissue.

Thermal, viscous, and compressibility effects were ignored, which invalidates the model only at very small diameters (a few micrometers), when implosion is rapid and internal pressure is high. The partial pressure of water in the bubble is taken to be the vapor pressure of water at ambient temperature. Its dependency on hydrostatic pressure and temperature is ignored, but these effects are significant only for tiny bubbles.

Similar assumptions are used in the Burkhard-Van Liew model (6), wherein the tissue-blood exchange is assumed to follow single-exponential kinetics, and gas concentration in the tissue is determined by assuming that the gas is uniformly distributed throughout the volume. However, the gas exchange between the bubble and tissue is determined from a steady-state solution to the diffusion equation with a source/sink term, but with no convective term. Their model does not incorporate CCE and uses an indirect method to calculate the partial pressure of CO_2 in the tissue.

Our model does incorporate the presence of the metabolic gases O_2, CO_2, and H_2O within the tissue and the bubble; the effect of a nonzero surface tension on the total pressure within the bubble; the consumption of O_2 and simultaneous generation of CO_2 within the tissue; the presence of dissolved CO_2 in the form of carbonic acid, bicarbonate, and carbonate; the effect of changes in hydrostatic pressure on bubble volume; the effects of CCE on inert gas uptake and elimination; and the complicated solubility curve for O_2 in whole blood. It is the most complete simulation of an extravascular bubble exposed to multiple gases of which we are aware.

RESULTS

For bubbles in adipose and spinal tissues, the simulated dive is to 75.9 and 69.3 fsw, respectively, for 4 h, with decompression stops at 66 fsw for 3 min, 33 fsw for 6 min, and 16.5 fsw for 11 min. Ascent rate was 39.4 fsw/min, and ascent time between stops is included in the time at a given stop (O. Hyldegaard, personal communication). The breathing gas was changed 30 min after surfacing to approximate the actual experimental conditions, and the initial bubble radius is taken to be ~3 μm for both tissues. These bubbles evolved to a maximum radius comparable to that observed experimentally. For bubbles in muscle and tendon, the simulated dive is to 82.5 fsw for 1 h, with 2-min decompression stops at 66, 33, and 16.5 fsw, with travel times of 15, 30, 15, and 30 s between stops, respectively. Gas switches for the muscle and tendon simulations occurred ~60 min after surfacing. Initial bubble radius for the muscle and tendon simulations was taken to be 290 μm. These bubbles grew, after decompression, to a radius of ~300 μm, corresponding to the size of the bubbles in the rat experiments.

Because bubbles in the experiments were generally isolated from other bubbles, we assumed a maximum bubble density of 1,000 bubbles/cm^3, corresponding to a spherical tissue volume of radius 0.06 cm. Simulations with larger and smaller volumes were also done, with the qualitative effects of gas switching being unaffected by the tissue volume. The diffusive time scale (length^2/distance) for this distance for all gases discussed here is on the order of 1–10 min. Distances to blood vessels (except in tendon) are more typically on the order of ≤100 μm, leading to diffusive time scales of at most a few tens of seconds. Table 1 shows the parameter values used for the simulations.

Figure 1 shows simulation results for a bubble evolving in spinal white matter. For the *top curves*, matching the experimental conditions of Hyldegaard et al. (19), the initial breathing gas is air. For the *bottom curves*, the breathing gas is 80% He-20% O_2. The simulation results indicate that for air and heliox breathing during the dive, switching the breathing gas to 100% O_2 is most effective at speeding dissolution of a bubble, and switching it to a heliox mixture is least effective. Delaying the gas switch did not change the qualitative effects of the switch.

Figure 2 shows similar results for a bubble evolving in adipose tissue. Again, switching the breathing gas to 100% O_2 is the most effective way to speed dissolution, and switching it to heliox is the least effective. For the air dives, the switch to heliox breathing initially speeds dissolution relative to air breathing but has the effect of slowing dissolution at later times. The initially beneficial effects of heliox breathing occur at 2–3 h after decompression, corresponding to the observation pe-

Table 1. *Simulation parameters*

	Adipose Tissue	Spinal White Matter	Muscle	Tendon
Diffusivity in tissue, 10^{-6} cm^2/s				
N_2	7.04 (18)	7.04 (18)	15.5*	15.5†
O_2	6.59 (18)	6.59 (18)	15.5 (21)	15.5†
CO_2	5.62 (18)	5.62 (18)	14.8 (21)	14.8†
He	18.6 (18)	18.6 (18)	40.0 (7, 20)	40.0†
Tissue-gas partition coeff, 10^{-6} $mol \cdot cm^{-3} \cdot atm^{-1}$				
N_2	2.557 (1)	0.6728 (1)	0.562 (35)	0.562 (35)
O_2	4.606 (1)	1.2330 (1)	1.070 (35)	1.070 (35)
CO_2	48.90 (1)	18.84 (1)	24.80 (35)	24.80 (35)
He	0.6431 (1)	0.2893 (1)	0.460 (35)	0.460 (35)
Blood-gas partition coeff, 10^{-6} $mol \cdot cm^{-3} \cdot atm^{-1}$				
N_2 (35)	0.5819	0.5819	0.5819	0.5819
CO_2 (27)	18.87	18.87	18.87	18.87
He (35)	0.3696	0.3696	0.3696	0.3696
Perfusion rate, vol blood·vol tissue^{-1}·min^{-1}	0.09 (24)	0.180 (13)	0.500 (11)	0.020‡
O_2 consumption rate, $cm^3 \cdot g^{-1} \cdot h^{-1}$ STP	0.112§ (4, 10,12)	0.684 (13)	0.450 (28)	0.030 (29)
Initial radius, μm	3	3	290	290

Numbers in parentheses are reference numbers. *Assumed to be the same as O_2. †Assumed to be the same as in muscle. ‡Estimated from data in other mammals. §Average of 3 values.

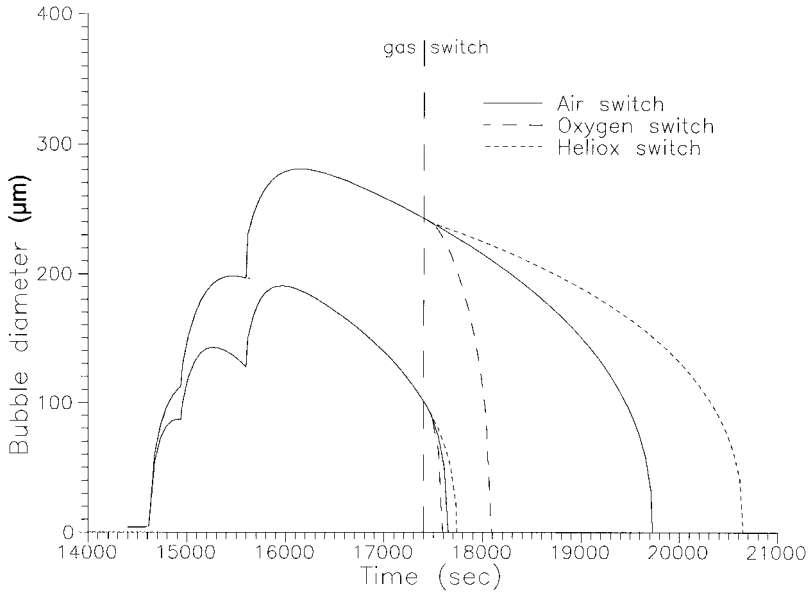

Fig. 1. Simulated effect of a breathing gas switch on growth of gas bubbles in rat spinal white matter. *Top curves* assume air breathing during dive; *bottom curves* assume heliox breathing during dive. A switch to O_2 breathing is most effective at reducing bubbles. Vertical dashed line, time of gas switch (30 min after surfacing).

riod of the rat experiments. In addition, the model predicts that bubbles in adipose tissue will persist for many hours longer than was observed experimentally.

Figures 3 and 4 show the simulation results for bubble evolution in muscle and tendon, respectively. Once again, the switch to O_2 is most effective in reducing the bubbles, and switches to heliox or air are less effective. In contrast to the situation in adipose tissue or spinal white matter, a switch to heliox breathing is slightly more effective at resolving bubbles than a switch to air breathing. These results are consistent, whether the diving gas is air or heliox.

DISCUSSION

Our simulations indicate that the heliox mixture may be the least effective of the three breathing gases modeled in resolving gas bubbles in spinal and adipose tissue and that O_2 breathing is much more effective in reducing bubbles than air or heliox breathing, irrespective of the tissue. What is the source of the discrepancy between the experimental results of Hyldegaard et al. (16, 17, 19) and the simulation results? Two possibilities are as follows: *1*) the physiological factors affecting bubble evolution in the tissue are affected by the dive, whether during the dive or after, and *2*) the transport of gases to the tissue is not described, as mentioned above, by the single-exponential function that can be determined from the tissue perfusion rate.

In *possibility 1* we include changes in O_2 consumption and tissue perfusion. During a dive the possibility exists that O_2 consumption and tissue perfusion are lower than on the surface, which leads to an effective increase in these factors on surfacing. After the dive, damage to the tissue or bubble growth in blood vessels may lead to a reduction in these factors. In *possibility 2* we include the process of CCE, wherein gas diffuses

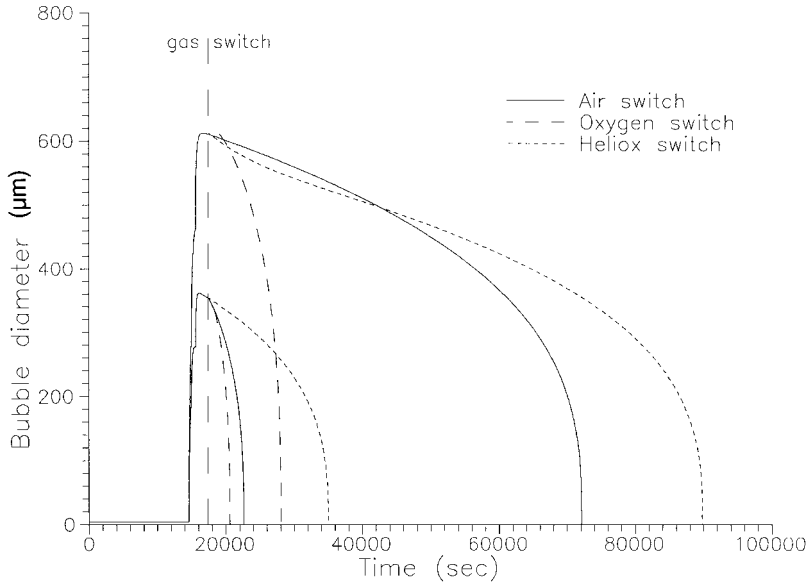

Fig. 2. Simulated effect of a breathing gas switch on growth of gas bubbles in rat adipose tissue. *Top curves* assume air breathing during dive; *bottom curves* assume heliox breathing during dive. A switch to O_2 breathing is most effective at reducing bubbles. Note transient period of growth of bubble after switch to O_2 breathing from breathing air; switch to heliox breathing is initially more effective at reducing bubbles than is continued breathing of air.

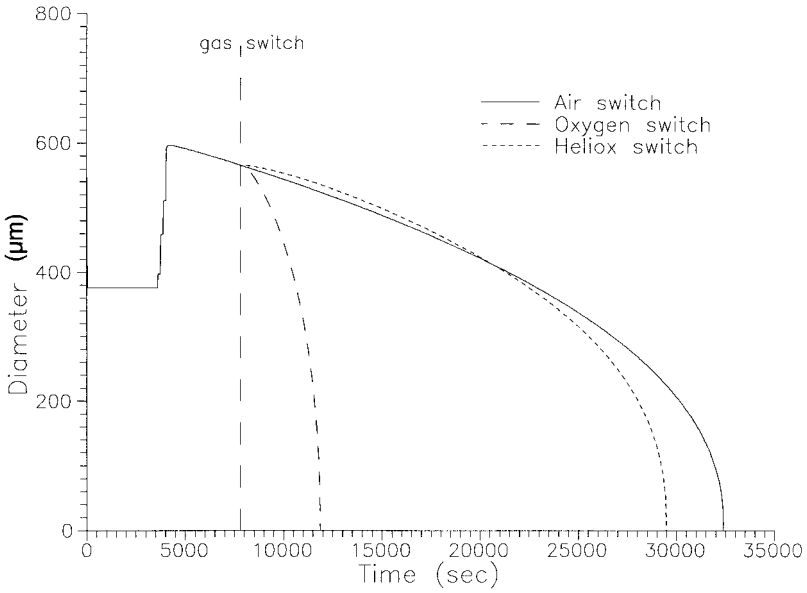

Fig. 3. Simulated effect of a breathing gas switch on growth of gas bubbles in rat muscle tissue after an air dive. A switch to O_2 breathing is most effective at reducing bubbles, and heliox breathing is slightly more effective at reducing bubbles than continued breathing of air. Curves for a heliox dive are very similar for bubble size and evolution.

between parallel blood vessels, leading to an effective lengthening of the tissue time constants for the gases. The amount of gas exchanged between the vessels will be greater for the more diffusible gases.

Figures 5 and 6 show simulation results for bubbles evolving in spinal white matter and in adipose tissue with the assumption of a 90% reduction in O_2 consumption rate that occurs at the same time as the gas switch. For the switch to pure O_2, a transient increase in bubble radius is observed, similar to that seen experimentally. Although lower O_2 consumption reproduces some aspects of bubble evolution seen experimentally, the qualitative aspects of bubble evolution (i.e., that switching the breathing gas to heliox is perhaps the least effective of the breathing gas switches in speeding bubble dissolution in fatty tissue) seem unaffected.

Simulation results for bubbles evolving in spinal white matter and adipose tissue with the assumption of an increase in O_2 consumption on surfacing (intended to simulate a possible suppression of O_2 consumption during the dive) indicate that bubble dissolution is speeded slightly, but the qualitative effects of the different gas switches are unchanged.

Another physiological factor that may be affected by decompression is the blood supply to the tissue. Changes in perfusion rate may also affect bubble evolution. Lowering the perfusion rate by 50% at the time of the gas switch slows the rate of dissolution slightly, and a 50% increase in perfusion speeds the rate of dissolution slightly, but the qualitative effects of the gas switches are again unchanged. A combination of increased O_2 consumption and increased perfusion speeds dissolution over that seen for either increase alone.

In *possibility 2*, where gas kinetics are not simply related to the tissue perfusion rate, we will assume that these effects are due to CCE. [There is evidence from experimental work and simulation that gas kinetics in

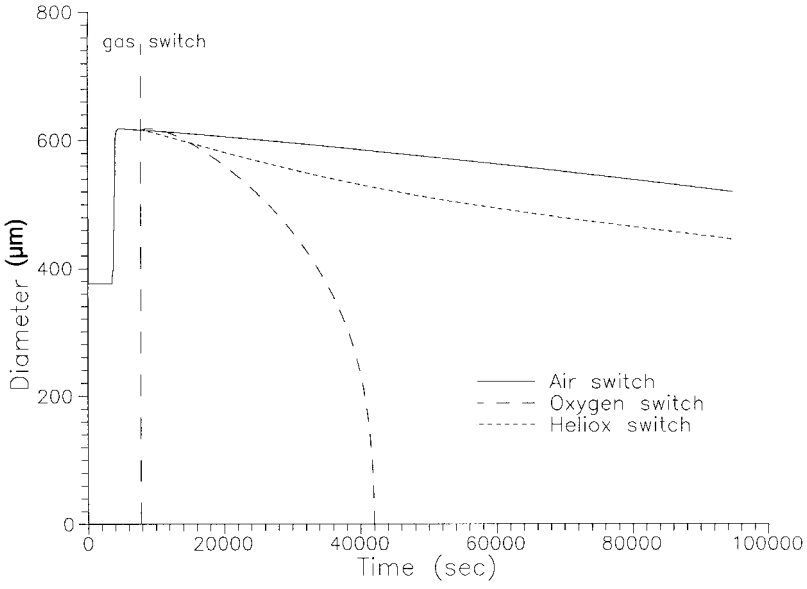

Fig. 4. Simulated effect of a breathing gas switch on growth of gas bubbles in rat tendon after an air dive. Curves for a heliox dive are very similar for bubble size and evolution. A switch to O_2 breathing is most effective at reducing bubbles, and heliox breathing is slightly more effective at reducing bubbles than is breathing of air.

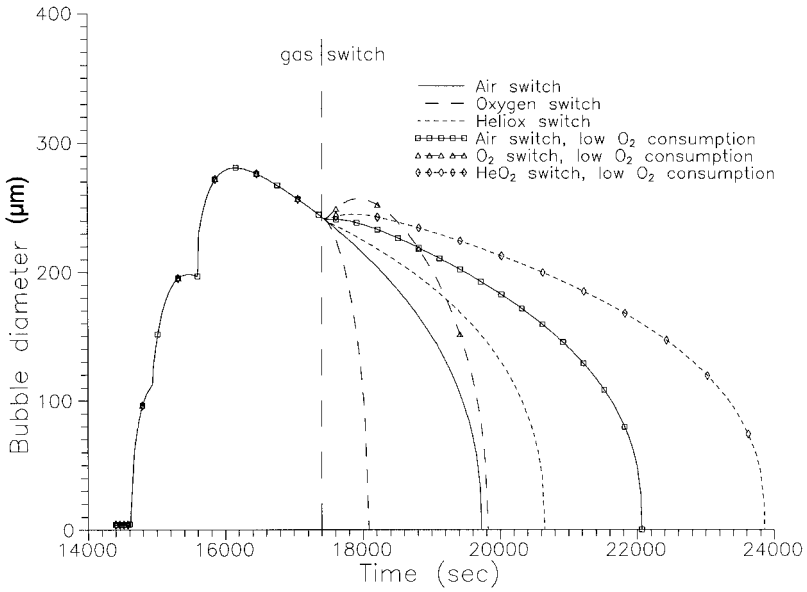

Fig. 5. Simulated effect of a breathing gas switch and a 90% reduction in O_2 consumption on evolution of gas bubbles. In rat spinal white matter, O_2 breathing is still most effective at resolving bubbles, but reduced O_2 consumption leads to a transient period of growth in bubble after switch in breathing gases.

tissue are not single exponential in nature. The experimental work of Novotny et al. (25) showed that xenon kinetics were not explained by a model of parallel compartments and that other factors, such as CCE or mixing between compartments, are important. The simulation work of Himm et al. (14) proposed that the relative dispersion in tissue transit times in rat muscle may be explained by assuming that there is mixing of inert gas between compartments. However, because data on the kinetics of gas washout in all these tissues are not available, we will use the simpler, single-exponential model.] To simulate the effects of CCE, the concentration of inert gas seen by the tissue is taken to be a weighted average of the concentration in the lung and the concentration in the tissue, as described in *Eq. 1*. O_2 is not subject to the CCE (15)

$$P^{a}_{i} = P^{l}_{i} + c_{\text{eff}} \cdot \frac{D_i}{D_0} \cdot (P^{ti}_{i} - P^{l}_{i}) \qquad (1)$$

where P^{l}_{i} is concentration of *gas i* in the lung, P^{ti}_{i} is concentration of *gas i* in the tissue, P^{a}_{i} is concentration of *gas i* in the blood supplying the tissue, c_{eff} is efficiency of the CCE process, D_i is diffusion coefficient of *gas i*, and D_0 is reference diffusion rate.

CCE of inert gases has the effect of delaying the washin and washout of inert gas in the tissue, thereby slowing the bubble evolution. The more diffusible a gas, the greater is the effective time constant for washout of the gas. The effect of CCE is illustrated in Figs. 7–10. Note the effect of the CCE in adipose tissue in Fig. 7.

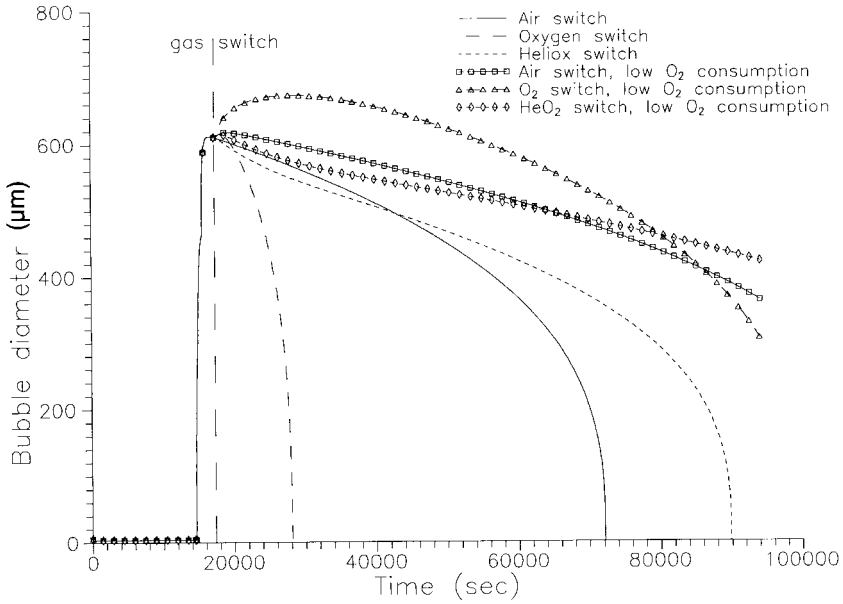

Fig. 6. In adipose tissue, reduction in O_2 consumption delays bubble resolution significantly, even though O_2 switch ultimately leads to most rapid resolution of bubble.

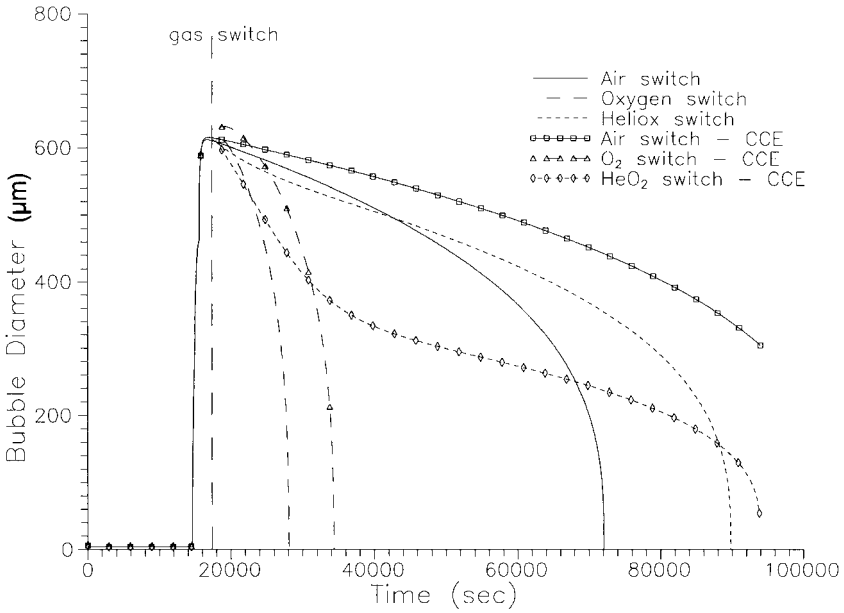

Fig. 7. Simulated effect of highly efficient (0.8) countercurrent exchange (CCE) on evolution of gas bubbles in adipose tissue. With this high level of CCE, heliox is initially more effective than O_2 at reducing bubbles and is more effective than continued breathing of air. Note more pronounced transient growth of bubble after switch to O_2.

Because air is used during the dive, CCE slows the washout of the N_2 from the tissue, so the bubble lifetime is ~50% longer. On switching the breathing gas to O_2, bubbles resolve most rapidly. However, the CCE of inert gases leads to a transient period of growth of the bubble. The switch to heliox leads to an initially faster rate of dissolution without CCE. With CCE, heliox breathing leads to a rapid decrease in size of the bubble initially and then a more gradual rate at later times, leading to complete resolution of the bubble in a shorter period of time than required during air breathing. In contrast, continued air breathing without CCE causes a more rapid resolution of the bubble.

Figure 8 shows the simulated effect of gas switching on the evolution of gas bubbles in spinal white matter. The dive simulated is similar to that for adipose tissue, 4 h at ~70 fsw, with a 20-min decompression. The breathing gas switch occurs 30 min after surfacing. The *bottom curves* show the effects of gas switching without CCE, and the *top curves*, with associated symbols, assume a $c_{eff} = 0.5$, which is a moderate level of CCE. With this moderate level of CCE, heliox breathing, although not as effective as O_2 breathing, is now more effective at resolving bubbles than continued air breathing. Again, this is in contrast to the simulated results without CCE.

Figures 9 and 10 show simulation results of the effect of breathing gas switches on bubble evolution in muscle and tendon, respectively. For these curves, $c_{eff} = 0.8$, which is a high degree of CCE. At this high level, a switch to heliox breathing is initially as effective as a switch to O_2 breathing, which leads to a very rapid resolution of the bubble. However, at longer times, the rate of bubble dissolution slows. Continued breathing of air is the least effective at resolving the bubble. These results are in contrast to the results without

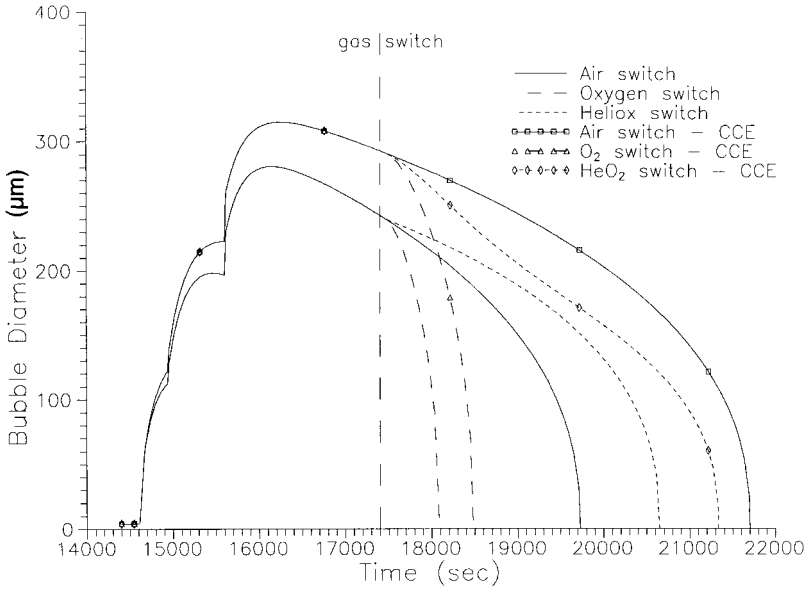

Fig. 8. Simulated effect of moderately efficient (0.5) CCE on evolution of gas bubbles in spinal white matter. With this level of CCE, heliox breathing is now more effective than air breathing at resolving air bubbles.

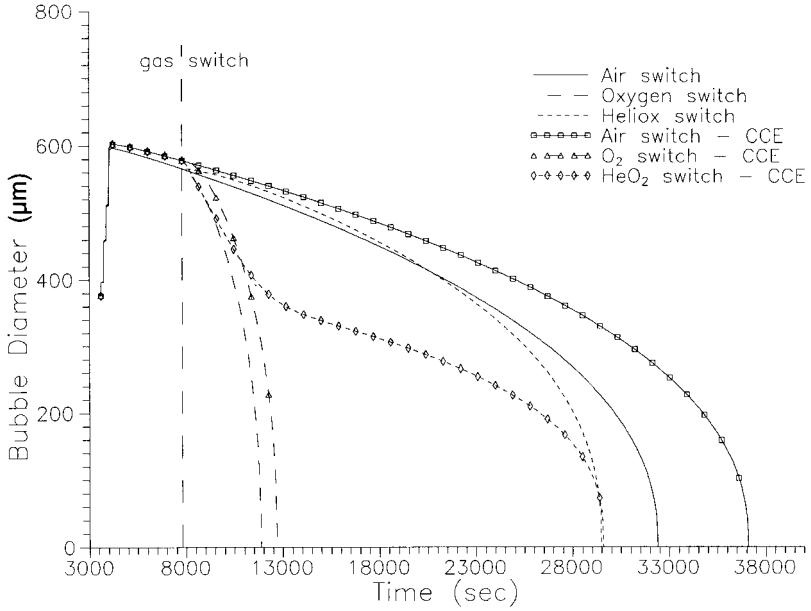

Fig. 9. Simulated effect of highly efficient (0.8) CCE on evolution of gas bubbles in muscle tissue. With this level of CCE, heliox breathing is initially as effective as O_2 at reducing bubbles.

CCE, where the switch to heliox breathing was only slightly more effective than continued breathing of air.

Conclusions. Because our model treats each tissue as a single well-mixed compartment, gas exchange between tissue and blood is probably more rapid in our model than in an actual tissue. We would expect bubble evolution in an actual tissue to proceed more slowly than modeled here, with the qualitative aspects being unaffected by the assumption of single-exponential kinetics for tissue-blood exchange. Our model reproduces qualitatively some aspects of the experimental results of Hyldegaard et al. (16, 17, 19) under the assumption of reduced O_2 consumption or CCE of inert gases but differs from the experimental results in some important ways, including which gas mixtures are best at resolving bubbles most rapidly. Possible sources of the discrepancies are mechanisms that may have effects similar to CCE, such as gas exchange with other tissue through which the arterial blood passes before it reaches the tissue of interest, or other tissue properties not accounted for here, such as tissue elasticity. An elastic response of the tissue, as in Gernhardt's model (9), would tend to increase the internal bubble pressure as the bubble grows, leading to more rapid dissolution of the bubble. Further experimental work, perhaps with heliox as the breathing gas during the dive, might help in determining the source of the discrepancies.

APPENDIX

For a single spherical bubble the mole flux of a *gas j* away from its surface is

$$J_j = k_j (C_j^{surf} - C_j^{\infty}) \quad (2)$$

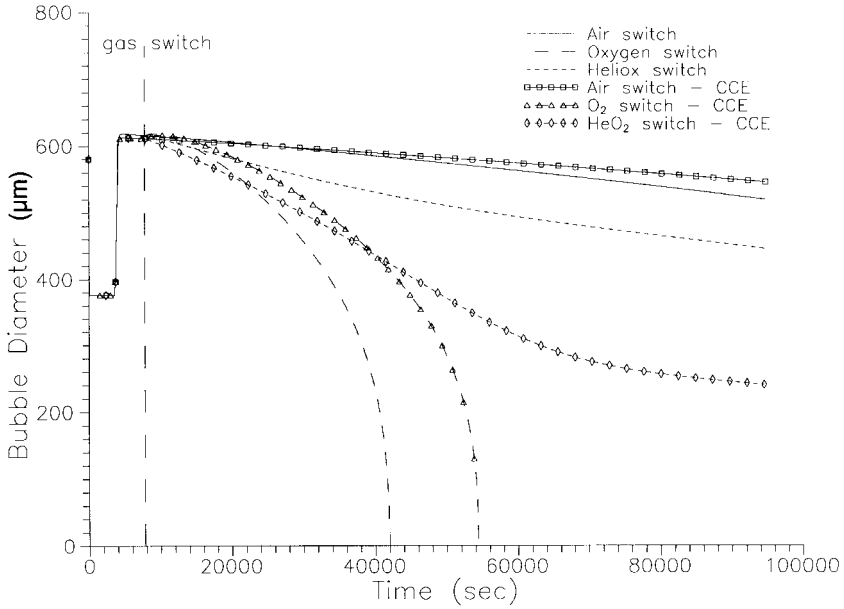

Fig. 10. Simulated effect of highly efficient (0.8) CCE on evolution of gas bubbles in tendon. Similar to bubble evolution in muscle at this level of CCE, heliox is initially as effective as O_2 and better than continued breathing of air.

where J_j is mole flux ($mol \cdot cm^{-2} \cdot s^{-1}$), k_j is external mass transfer coefficient (cm/s), C_j^{surf} is concentration of dissolved gas at the outer bubble surface (mol/cm^3), and C_j^{∞} is concentration of dissolved gas far from the surface (mol/cm^3).

We make the following assumptions: *1*) There is equilibrium between phases across the phase interface. *2*) There is no resistance to mass transport in the gas phase; therefore, the partial pressure of each gas at the inner bubble surface (P^{surf}) equals its bulk value (P^{bub}) in the bubble. *3*) Henry's law applies to each dissolved gas; i.e., the concentration of each dissolved gas (C_{dis}) is proportional to the partial pressure of gas with which it would be in equilibrium (P_{dis}), with the proportionality factor being a concentration-independent solubility or partition coefficient (K)

$$C_{dis} = K^{ti\text{-}gas} P_{dis}$$

Equation 1 now becomes

$$J_j = k_j K_j^{ti\text{-}gas} (P_j^{bub} - P_j^{\infty}) \tag{3}$$

where K_j is the tissue-gas partition coefficient ($mol \cdot cm^{-3} \cdot atm^{-1}$). Mechanical equilibrium at the phase boundary requires that when the hydrostatic pressure within the bubble equals the sum of the partial pressures of all gases in the bubble

$$\Sigma P_j^{bub} = \rho + 2\sigma/R - P_{H_2O} \tag{4}$$

where ρ is ambient hydrostatic pressure (dyn/cm^2) and σ is surface tension (dyn/cm).

The above summation is over j, and partial pressure of H_2O (P_{H_2O}) is taken as constant. The mass balance on the gas inside the bubble (with the assumption of sphericity) gives

$$J_j = \frac{1}{4\pi R^2} \frac{d n_j^{bub}}{dt} \tag{5}$$

where R is bubble radius (cm) and n_j^{bub} is number of moles of *gas j* inside the bubble.

Assuming ideal gases, we have

$$n_j^{bub} = \frac{4\pi R^3 P_j^{bub}}{3R_G T} \tag{5a}$$

$$\Sigma n_j^{bub} = \frac{4\pi R^3}{3R_G T} \Sigma P_J^{bub} \tag{5b}$$

which can be rewritten using *Eq. 3* as

$$\Sigma n_j^{bub} = \frac{4\pi R^3}{3R_G T} (\rho + 2\sigma/R - P_{H_2O}) \tag{5c}$$

where R_G is gas law constant ($82.057\ atm \cdot cm^3 \cdot mol^{-1} \cdot °K^{-1}$) and T is absolute temperature (°K).

Differentiation of *Eq. 5c* with respect to time yields

$$d(\Sigma n_j^{bub})/dt = \Sigma dn_j^{bub}/dt = \frac{4\pi}{R_G T}\left\{\left[(\rho - P_{H_2O})R^2 + \frac{4R\sigma}{3}\right]\frac{dR}{dt} + \frac{R^3}{3}\frac{d\rho}{dt}\right\} \tag{6}$$

Equations 2, *4*, and *6* are combined to yield

$$\frac{dR}{dt} = -\frac{R_G T \Sigma[k_j K_j^{ti\text{-}gas} (P_j^{bub} - P_j^{\infty})] + \frac{R}{3}\frac{d\rho}{dt}}{\left(\rho - P_{H_2O} + \frac{4\sigma}{3R}\right)} \tag{7}$$

For the mass transfer coefficient, we use the result that for a sphere in a quiescent liquid the dimensionless Sherwood number (Sh) is 2.0 (31), so for any of the *gases j*

$$Sh = 2.0 = \frac{2R k_j}{D_j}$$

or

$$k_j = D_j/R \tag{8}$$

where D is the diffusivity (cm^2/s). Substitution into *Eq. 7* results in the final form of the equation for the rate of change of the bubble radius

$$\frac{dR}{dt} = -\frac{R_G T \Sigma[D_j K_j (P_j^{bub} - P_j^{\infty})] + \frac{R^2}{3}\frac{d\rho}{dt}}{R\left(\rho - P_{H_2O} + \frac{4\sigma}{3R}\right)} \tag{9}$$

An expression for dP_j^{∞}/dt is also necessary. To obtain it, first note that a mass balance around the finite closed system shows that

$$\frac{dC_j^{\infty}}{dt} = K_j^{ti\text{-}gas}\frac{dP_j^{\infty}}{dt} = -\frac{1}{V_l}\frac{dn_j^{bub}}{dt} \tag{10}$$

where V_l is the volume of the condensed phase (cm^3). An expression for dn_j^{bub}/dt is acquired by differentiating *Eq. 5a*

$$\frac{dn_j^{bub}}{dt} = \frac{4\pi}{3R_G T}\left(3P_j^{bub} R^2 \frac{dR}{dt} + R^3 \frac{dP_j^{bub}}{dt}\right) \tag{11}$$

This is substituted into *Eq. 10* to yield

$$\frac{dP_j^{\infty}}{dt} = \frac{4\pi}{3V_l K_j^{ti\text{-}gas} R_G T}\left(3P_j^{bub} R^2 \frac{dR}{dt} + R^3 \frac{dP_j^{bub}}{dt}\right) \tag{12}$$

If the system is open to mass transport, then dissolved gas is exchanged with the surroundings of the volume element, which in this case is arterial blood. If the tissue is treated as a well-mixed compartment with a constant tissue-blood partition coefficient, then the kinetics of this exchange are single exponential and *Eq. 12* becomes

$$\frac{dP_j^{\infty}}{dt} = \frac{P_j^{art} - P_j^{\infty}}{\tau_j} - \frac{4\pi}{3V_l K_j^{ti\text{-}gas} R_G T}\left(3P_j^{bub} R^2 \frac{dR}{dt} + R^3 \frac{dP_j^{bub}}{dt}\right) \tag{13}$$

Here, P_j^{art} is the tension of *gas j* in arterial blood and τ_j is the time constant for exchange of *gas j* between tissue and blood, given by

$$\tau_j = \frac{K_j^{ti\text{-}blood}}{F} \tag{14}$$

where $K_j^{ti\text{-}blood}$ is tissue-blood partition coefficient for *gas j* $[[mol \cdot (cm^3\ tissue)^{-1}] \cdot [mol \cdot (cm^3\ blood)^{-1}]^{-1}]$, equal to the ratio of the solubility in tissue to the solubility in blood ($K_j^{ti\text{-}gas}/K_j^{blood\text{-}gas}$) and F is specific rate of perfusion ($cm^3\ blood \cdot cm^3\ tissue^{-1} \cdot s^{-1}$).

For all gases except O_2, the arterial gas tensions in the lung are computed from the breathing gas composition by applying the usual correction for the presence of water vapor and CO_2. The effects of CCE are simulated by shifting the arterial gas tensions from the value in the lung toward the gas tension in

the tissue. The magnitude of the shift is larger for the more diffusible gases and is given by

$$P_j^{art} = P_j^{lung} + \epsilon \frac{D_j}{D_{ref}} (P_j^{\infty} - P_j^{lung}) \quad (15)$$

where $0 < \epsilon < 1$ is a factor describing the efficiency of the CCE process for a reference gas with diffusion coefficient D_{ref}. No CCE is described by $\epsilon = 0$, whereas perfect exchange is given by $\epsilon = 1$. The arterial O_2 tension is computed after West (37). For O_2 the tissue-blood exchange is a bit different, because its solubility in blood is not concentration independent, and hence the tissue-blood partition coefficient is not constant. The Hill equation [$P_{50} = 36$ Torr, $n = 2.6$ (8), where P_{50} is O_2 half-saturation pressure of Hb and n is Hill's coefficient] was used to determine the O_2 concentration in blood as a function of its partial pressure and was used to obtain the partition coefficient as a function of P_{ox}^{blood}

$$K_{ox}^{blood\text{-}gas}(P_{ox}^{blood}) = \frac{C_{ox}^{blood}}{P_{ox}^{blood}} \quad (16)$$

Also, for O_2 there is an additional term on the right-hand side of *Eq. 13* that accounts for metabolic consumption. Incorporating these refinements into *Eq. 13* as written for O_2 results in

$$\frac{dP_{ox}^{\infty}}{dt} = -\frac{R_{ox}}{K_{ox}^{ti\text{-}gas}} + \frac{F}{K_{ox}^{ti\text{-}gas}}[K_{ox}^{blood\text{-}gas}(P_{ox}^{art})P_{ox}^{art} - K_{ox}^{blood\text{-}gas}(P_{ox}^{\infty})P_{ox}^{\infty}] - \frac{4\pi}{3V_l K_{ox}^{ti\text{-}gas} R_G T}\left(3P_{ox}^{bub} R^2 \frac{dR}{dt} + R^3 \frac{dP_{ox}^{bub}}{dt}\right) \quad (13')$$

Here, R_{ox} is the rate of O_2 consumption per unit volume ($mol \cdot cm^{-3} \cdot s^{-1}$) and is believed to be independent of O_2 tension in adipose and spinal nerve tissue. Similarly, for CO_2 there is a term accounting for metabolic generation

$$\frac{dP_{CO_2}^{\infty}}{dt} = RQ\frac{R_{ox}}{K_{CO_2}^{ti\text{-}gas}} + \frac{P_{CO_2}^{art} - P_{CO_2}^{\infty}}{\tau_{CO_2}} - \frac{4\pi}{3V_l K_{CO_2}^{ti\text{-}gas} R_G T}\left(3P_{CO_2}^{bub} R^2 \frac{dR}{dt} + R^3 \frac{dP_{CO_2}^{bub}}{dt}\right) \quad (13'')$$

where RQ is the respiratory quotient (mol CO_2/mol O_2).

To describe the system we still require an independent expression for dP_j^{bub}/dt. To obtain it, the rate-related *Eqs. 2*, *4*, and *8* are combined with the mass balance of *Eq. 11* to yield the expression

$$\frac{dP_j^{bub}}{dt} = \frac{3D_j K_j^{ti\text{-}gas} R_G T}{R^2}(P_j^{\infty} - P_j^{bub}) - \frac{3P_j^{bub}}{R}\frac{dR}{dt} \quad (17)$$

Equations 9, *13*, and *17* are independent and define the system. For n diffusing gases, there are $(2n + 1)$ equations.

One additional detail will be noted regarding the partitioning of CO_2. The CO_2 gas is equilibrated with the dissolved CO_2 across the phase interface according to

$$C_{CO_2}(aq) = K_{CO_2}^{ti\text{-}gas} P_{CO_2} \quad (18)$$

where $C_{CO_2}(aq)$ is the concentration of unhydrated dissolved CO_2. The unhydrated CO_2 exchanges with carbonic acid, bicarbonate, and carbonate

$$CO_2(aq) + H_2O \rightleftharpoons H_2CO_3 \rightleftharpoons HCO_3^- + H^+ \rightleftharpoons CO_3^{2-} + 2H^+ \quad (19)$$

The equilibrium coefficients are defined as follows

$$\alpha_2 = \frac{[H_2CO_3]}{[CO_2(aq)][H_2O]} \quad (20a)$$

$$\alpha_3 = \frac{[HCO_3^-][H^+]}{[H_2CO_3]} \quad (20b)$$

$$\alpha_4 = \frac{[CO_3^{2-}][H^+]}{[HCO_3^-]} \quad (20c)$$

where the square brackets denote molar concentrations (mol/l). The fraction (frac) of the total dissolved CO_2 that is undissociated at equilibrium is found to be

$$frac = \frac{1}{1 + \alpha_2[H_2O] + \alpha_2\alpha_3\frac{[H_2O]}{[H^+]} + \alpha_2\alpha_3\alpha_4\frac{[H_2O]}{[H^+]^2}} \quad (21)$$

In the calculations for CO_2 it is assumed that the unhydrated form is equilibrated with the other forms, and the total dissolved CO_2 is quantified by using "effective" values of the tissue-gas and blood-gas partition coefficients to account for the fact that only a fraction of the dissolved CO_2 shows up as CO_2(aq), as follows

$$K_{eff} = \frac{K}{frac} \quad (22)$$

The molar concentration of protons at physiological pH is of course

$$[H^+] = 10^{-7.4}$$

At pH 7.4 it is calculated that frac has a value of only 0.0016. Consequently, the effective tissue-gas partition coefficient is high enough to make the tissue an efficient sink/source of CO_2, and it is found that the tension of dissolved CO_2 is essentially a constant 0.0461 ATA.

The authors are grateful to Dr. G. Albin for invaluable scientific contribution to this paper.

This work was supported by Naval Medical Research and Development Command Work Unit 62233N MM33P30.004-1509.

The opinions and assertions contained herein are the private ones of the authors and are not to be construed as official or reflecting the views of the US Navy or the naval service at large.

Address for reprint requests and other correspondence: J. F. Himm, Code 31, Diving and Environmental Physiology Dept., Naval Medical Research Institute, 8901 Wisconsin Ave., Bethesda, MD 20889-5607 (E-mail: himmj@nmripo.nmri.navy.mil).

Received 19 February 1997; accepted in final form 14 May 1999.

REFERENCES

1. **Abraham, M. H., M. J. Kamlet, R. W. Taft, R. M. Doherty, and P. K. Weathersby.** Solubility properties in polymers and biological media. 2. The correlation and prediction of the solubilities of nonelectrolytes in biological tissues and fluids. *J. Med. Chem*. 28: 865–870, 1985.
2. **Ball, R., J. F. Himm, L. D. Homer, and E. D. Thalmann.** *A Model of Bubble Evolution During Decompression Based on a Monte Carlo Simulation of Inert Gas Diffusion*. Bethesda, MD: Naval Medical Research Institute, 1994. (NMRI Rep. 94-36)

3. **Ball, R., J. F. Himm, L. D. Homer, and E. D. Thalmann.** Does the time course of bubble evolution explain decompression sickness risk? *Undersea Hyperb. Med*. 22: 263–280, 1995.
4. **Bray, G. A., and H. M. Goodman.** Metabolism of adipose tissue from normal and hypothyroid rats. *Endocrinology* 82: 860–864, 1968.
5. **Brian, P. L. T., and H. B. Hales.** Effects of transpiration and changing diameter on heat and mass transfer to spheres. *AIChE* 15: 419–435, 1969.
6. **Burkard, M. E., and H. D. Van Liew.** Simulation of exchange of multiple gases in bubbles in the body. *Respir. Physiol*. 95: 131–145, 1994.
7. **Carles, A. C., T. Kawashiro, and J. Piiper.** Solubility of various inert gases in rat skeletal muscle. *Pflügers Arch*. 359: 209–218, 1975.
8. **Cartheuser, C. F.** Standard and pH-affected hemoglobin-O_2 binding curves of Sprague-Dawley rats under normal and shifted P_{50} conditions. *Comp. Biochem. Physiol. A Physiol*. 106: 775–782, 1993.
9. **Gernhardt, M. L.** *Development and Evaluation of a Decompression Stress Index Based on Tissue Bubble Dynamics* (Ph.D. dissertation). Philadelphia, PA: University of Pennsylvania, 1991.
10. **Giudicelli, Y., R. Nordmann, and J. Nordmann.** Metabolic effects of acetaldehyde on rat adipose tissue. *Biochim. Biophys. Acta* 280: 393–407, 1972.
11. **Gorski, J., D. A. Hood, and L. Terjung.** Blood flow distribution in tissues of perfused rat hindlimb preparations. *Am. J. Physiol*. 250 (*Endocrinol. Metab*. 13): E441–E448, 1986.
12. **Hallgren, P., S. Korsback, and L. Sjostrom.** Measurements of adipose tissue respiration in a closed chamber using an oxygen sensor: methodological considerations. *J. Lipid Res*. 27: 996–1005, 1986.

12a. **Halpern, D., Y. Jiang, and J. F. Himm.** Mathematical model of gas bubble evolution in a straight tube. *J. Biomechc. Eng.* In press.

13. **Hayashi, N., B. A. Green, M. Gonzalez-Carvajal, J. Mora, and R. P. Veraa.** Local blood flow, oxygen tension, and oxygen consumption in the rat spinal cord. 2. Relation to segmental level. *J. Neurosurg*. 58: 526–530, 1983.
14. **Himm, J. F., L. D. Homer, and J. A. Novotny.** Effect of lipid on inert gas kinetics. *J. Appl. Physiol*. 77: 303–312, 1994.
15. **Honig, C. R., T. E. J. Gayeski, A. Clark, and P. A. A. Clark.** Arteriovenous oxygen diffusion shunt is negligible in resting and working gracilis muscles. *Am. J. Physiol*. 261 (*Heart Circ. Physiol*. 30): H2031–H2043, 1991.
16. **Hyldegaard, O., and J. Madsen.** Influence of heliox, oxygen, and N_2O-O_2 breathing on N_2 bubbles in adipose tissue. *Undersea Biomed. Res*. 16: 185–193, 1989.
17. **Hyldegaard, O., and J. Madsen.** Effect of air, heliox, and oxygen breathing on air bubbles in aqueous tissues in the rat. *Undersea Hyperb. Med*. 21: 413–424, 1994.
18. **Hyldegaard, O., and J. Madsen.** Effect of SF_6-O_2 breathing on air bubbles in rat tissues. *Undersea Hyperb. Med*. 22: 355–365, 1995.
19. **Hyldegaard, O., M. Moller, and J. Madsen.** Effect of He-O_2, O_2, and N_2O-O_2 breathing on injected bubbles in spinal white matter. *Undersea Biomed. Res*. 18: 361–371, 1991.
20. **Kawashiro, T., A. C. Carles, S. F. Perry, and J. Piiper.** Diffusivity of various inert gases in rat skeletal muscle. *Pflügers Arch*. 359: 219–230, 1975.
21. **Kawashiro, T., W. Nusse, and P. Scheid.** Determination of diffusivity of oxygen and carbon dioxide in respiring tissue: results in rat skeletal muscle. *Pflügers Arch*. 359: 231–251, 1975.
22. **Kislyakov, Y. Y., and A. V. Kopyltsov.** The rate of gas-bubble growth in tissue under decompression. Mathematical modeling. *Respir. Physiol*. 71: 299–306, 1988.
23. **Kol, S., Y. Adir, C. R. Gordon, and Y. Melamed.** Oxy-helium treatment of severe spinal decompression sickness after air diving. *Undersea Hyperb. Med*. 20: 147–154, 1993.
24. **Larsen, T., K. Myhre, H. Vik-mo, and O. D. Mjos.** Adipose tissue perfusion and fatty acid release in exercising rats. *Acta Physiol. Scand*. 113: 111–116, 1981.
25. **Novotny, J. A., D. L. Mayers, Y. F. Parsons, S. S. Survanshi, P. K. Weathersby, and L. D. Homer.** Xenon kinetics in muscle are not explained by a model of parallel perfusion-limited compartments. *J. Appl. Physiol*. 68: 876–890, 1990.

25a. **Parker, E. C., S. S. Survanshi, P. B. Massell, and P. K. Weathersby.** Probabilistic models of the role of oxygen in human decompression sickness. *J. Appl. Physiol*. 84: 1096–1102, 1998.

26. **Parker, E. C., S. S. Survanshi, P. K. Weathersby, and E. D. Thalmann.** *Statistically Based Decompression Tables. VIII. Linear-Exponential Kinetics*. Bethesda, MD: Naval Medical Research Institute, 1992.
27. **Prosser, C. L.** Oxygen: respiration, and metabolism. In: *Comparative Animal Physiology*, edited by C. L. Prosser. Philadelphia, PA: Saunders, 1973, p. 165–211.
28. **Ruderman, N. B., F. W. Kemmer, M. N. Goodman, and M. Berger.** Oxygen consumption in perfused skeletal muscle. *Biochem. J*. 190: 57–64, 1980.
29. **Sommer, H. M.** The biomechanical and metabolic effects of a running regime on the Achilles tendon in the rat. *Int. Orthop*. 11: 71–75, 1987.
30. **Tikuisis, P., K. Gault, and G. Carrod.** Maximum likelihood analysis of bubble incidence for mixed gas diving. *Undersea Biomed. Res*. 17: 159–169, 1990.
31. **Treybal, R. E.** *Mass Transfer Operations*. New York: McGraw-Hill, 1979.
32. **Van Liew, H. D.** Simulation of the dynamics of decompression sickness and the generation of new bubbles. *Undersea Biomed. Res*. 18: 333–345, 1991.
33. **Van Liew, H. D., and M. E. Burkard.** Bubbles in circulating blood: stabilization and simulations of cyclic changes of size and content. *J. Appl. Physiol*. 79: 1379–1385, 1995.
34. **Ward, C. A., P. Tikuisis, and R. D. Venter.** Stability of bubbles in a closed volume of liquid-gas solution. *J. Appl. Physiol*. 53: 6076–6084, 1982.
35. **Weathersby, P. K., and L. D. Homer.** Solubility of inert gases in biological fluids and tissues: a review. *Undersea Biomed. Res*. 7: 277–296, 1980.
36. **Weathersby, P. K., S. S. Survanshi, L. D. Homer, E. C. Parker, and E. D. Thalmann.** Predicting the time of occurrence of decompression sickness. *J. Appl. Physiol*. 72: 1541–1548, 1992.
37. **West, J. B.** *Respiratory Physiology*. Baltimore, MD: Williams & Wilkins, 1985.